Evaluation of the Processing Parameters Influence on the Additive Manufacturing of VP50IM Steel by PCGTAW

Paulo Henrique Toaldo[1] , Arthur Soares Fernandes Ferreira[1] , Roger Navarro Verastégui[1] , Anderson Geraldo Marenda Pukasiewicz[1]

[1] Universidade Tecnológica Federal do Paraná – UTFPR, Ponta Grossa, PR, Brasil.

Abstract: The wire arc additive manufacturing process or WAAM (Wire Additive Arc Welding) is recognized as a process able of making pieces of high geometric complexity, with mechanical properties comparable to those of the cast material. However, there are significant challenges associated with WAAM, such as undesirable microstructures and mechanical properties, high residual stresses and geometric distortion. This study aims to contribute to the selection of deposition parameters for VP50IM steel using WAAM via pulsed TIG (Tungsten Inert Gas) and characterization of the generated stacking, using the Central Composite Complete methodology, CCC. In this study, the peak (Cp) and base (Cb) current, wire feed speed during peak (Vap), base (Vab) and welding speed (Vs) were varied. The ideal parameter presented was Cp=200A, Cb=100A, Vap=2.9cm/min, Vab=1.2cm/min and Vs=20cm/min. Tensile tests showed up to 15% greater resistance in the samples in the longitudinal section in the welding direction compared to the transverse direction. Hardness tests demonstrated up to 9% less hardness at the center of the stack compared to the top and bottom. The fracture analysis of the specimens showed ductile fracture.

Key-words: Welding; Additive manufacturing; VP50IM; GTAW pulsed; Forming profile.

Avaliação da Influência dos Parâmetros de Processamento na Manufatura Aditiva do Aço VP50IM por PCGTAW

Resumo: O processo de manufatura aditiva a arco arame ou WAAM (*Wire Additive Arc Welding*) é reconhecido como um processo capaz de confeccionar peças de elevada complexidade geométrica, com propriedades mecânicas comparáveis às do material fundido. Entretanto, existem desafios significativos associados ao WAAM, como microestruturas e propriedades mecânicas indesejáveis, elevadas tensões residuais e distorção geométrica. Este estudo visa contribuir com a seleção de parâmetros de deposição do aço VP50IM utilizando WAAM via TIG (*Tungsten Inert Gas*) pulsado e caracterização do empilhamento gerado, utilizando a metodologia Central Composto Completo, CCC. Neste estudo variou-se a corrente de pico (Cp) e de base (Cb), velocidade de alimentação de arame durante pico (Vap), base (Vab) e velocidade de soldagem (Vs). O parâmetro ideal apresentado foi Cp=200A, Cb=100A, Vap=2,9cm/min, Vab=1,2cm/min e Vs=20cm/min. Ensaios de tração mostraram uma resistência até 15% maior nas amostras na seção longitudinal ao sentido de soldagem em comparação ao sentido transversal. Ensaios de dureza demonstraram uma dureza até 9% menor no centro do empilhamento em comparação ao topo e base. A análise de fratura dos corpos de prova evidenciou fratura dúctil.

Palavras-chave: Soldagem; Manufatura aditiva; VP50IM; GTAW pulsado; Formação de perfil.

1. Introduction

The manufacturing of goods, as one of the pillars of society's development, has always attracted the attention of researchers and professionals from different areas of knowledge, due to its multidisciplinary characteristics. The traditional methods of producing include casting, forming, welding and machining processes and their variations. However, these conventional processes, even though they are currently reduced, still produce a high amount of waste and a high quantity of material, energy and inventory loss, contributing negatively to the environment, due to the generation of contaminants and excess materials by using a subtractive manufacturing methodology [1,2].

As an option, the additive manufacturing methodology has gained the media and industry spotlight with the expression "3D printing", having a substantial development from the 1980s until today [3]. There are several terms found to identify Manufacturing, due to the revolution we are experiencing, but it was the term Additive Manufacturing (AM) which characterizes the group of technologies that uses a layer-by-layer approach to create functional components, with free form; from bottom to top, giving physical form to a 3D model previously developed in a digital file [1,2,4].

Allied to welding processes, AM enters the scene with several processes, including Wire Arc Additive Manufacturing (WAAM), a more environmentally friendly method as it does not expose the environment and operators to the presence of potentially dangerous

dust, material widely used in laser additive manufacturing for example. The WAAM method has greater deposition efficiency, as the use of wire presents a deposition efficiency close to 100% of the wire material used [5], and this technique belong to the Direct Energy Deposition (DED) category as described by the ISO/ASTM 52900:2015(E) [4]. WAAM is an ideal additive manufacturing process for manufacturing large-scale or large-format parts efficiently and cost-effectively compared to other AM methods, finding applications in diverse fields including aerospace, automotive and molds [6,7]. Different welding processes such as Gas Metal Arc Welding (GMAW) [8], Gas Tungsten Arc Welding (GTAW) [9], Plasma Arc Welding (PAW) [10] are commonly used as WAAM technique.

Accurate prediction of WAAM part dimension mainly depends of the deposition parameters control [9], and the modeling of the single bead profile and its subsequent overlaps [11]. A profile-transformed recursive model was then formulated and explained in detail in Chen et al. [12]. Other deposition modeling was proposed in Ding et al. [5], where the tangent overlap model (TOM) is established, and the concept of the critical central distance for stable multi-granule overlap processes is presented. The proposed TOM provides a much better approximation to experimental measurements when compared to the traditional flat-top overlay model (FOM). The improvement of the dimension control can also achieve by an electromagnetic arc constriction as proposed in Antonello et al. [13]. Mechanical properties is another important aspect that must to be considered during the use of WAAM technique to generate different components. The control of the WAAM mechanical and microstructural properties can be achieve by different ways, like arc metal-transfer control [8], laser-arc hybrid additive manufacturing [14], deposition process parameters [9,15,16], equivalent heat input control [17,18], pulsed-arc plasma control [10], and the use of heat treatments after deposition [19].

In additive manufacturing of tool steels, it is necessary to control some primary parameters, like welding current and voltage, as well as wire feeding rate, wich control the heat input of the deposition [15], and non-primary parameters, such as pre-heating and interpass temperature [20]. Despite not being a parameterized variable directly in a machine, studies [9,20-23] demonstrate that the variation in temperature or time of the interpass has an influence on the grain size generated during solidification, due to the change in the intrinsic treatment that occurred, changing the generated microstructure and the mechanical properties of the final part. A methodology adopted by researchers [9,21-23] to face such challenges are studies that improve the AM technique with the characterization of weld bead profiles, making it possible to understand the welding characteristics with greater precision in their properties.

The tensile properties obtained from WAAM of high resistant steel like Maraging or Hot Work Steel like H11 and H13 are similar than bulk conventional hot forging ones [15,18], as well as fatigue resistance in ER100S-G steel that showed high fatigue resistance for WAAM specimens [24]. Higher wear resistance was also achieve in submerged arc welding in H13 [25]. Lower toughness, around 70-85% of the H11 was observed in WAAM deposited samples [15]. However promising toughness values in WAAM Inconel 718 was observed before and after heat treatment, showing 100% higher toughness value than standard HT Inconel 718 sample [19]. This remarkable result was explained by the authors by the single step age hardening, which avoid the full precipitation of γ' and γ" phases, improving the mechanical strength, maintaining soft matrix and good ductility of parts [19]. Different deposition methods were also evaluated in H13 Hot Working Tool Steel, showing that these different processes can achieve high quality and similar mechanical properties than H13 bulk steel [20].

Additive manufacturing technology can contribute significantly with the development of new molds and dies, and this work contribute with the development of this technology studying the influence of the deposition parameters on the construction of a profile by WAAM manufacture using Pulsed Gas-Tungsten Arc Welding (PGTAW) to deposit VP50IM tool steel thin walls. The experiment was conducted through analysis of the microstructure and mechanical properties of the material deposited layer by layer, following the CCC (Complete Composite Central) methodology. This methodology contributes to the scientific community with an analysis of the influence of the deposition parameters of a profile made by AM, optimizing welding parameters to improve the geometry quality observed by visual inspection, cross-section geometry, dilution and wettability. The influence of the deposited material orientation on the tensile strength were also evaluated through a tensile test, evaluating the deposition effect on the mechanical properties anisotropy.

2. Materials and Methods

2.1. Materials

The material used for deposition was solid wire VH50IM, 1.2 mm in diameter, with chemical composition shown in Table 1. To evaluate the chemical composition presents in the deposited material, an energy dispersion spectroscopy (EDS) semi-quantitative analysis was used.

Table 1. Chemical composition measured by EDS of the wire filler steel (1.2mm wire).

Chemical Element	Ni	Mn	Si	Cr	Mo
wt [%]	2.7	1.8	0.9	0.3	0.3

In AM processes, it is common for the final part to be independent of the metal that was used to start the process, that is, to discard the base metal. Thus, it was decided to use a material that is easy to obtain commercially, using carbon steel SAE 1020.

2.2. Equipaments and deposition set-up

An IMC® DIGIplus A7 ACPO3C Multiprocess welding machine was used. The displacement of the torch during welding was carried out by the Tartílope V1 equipment, capable of moving at constant speed in the X axis, allowing uniform welding longitudinally. Pulsed Gas tungsten arc welding process was selected in this research to be used as WAAM process. GTAW consist of a well-controlled metal transfer, which possibility an important reduction on the welding defects. Compared with Gas metal arc welding (GMAW), GTAW presents lower deposition rate, but has a more stable process.

A two-stage experiment was designed to study the parameters effects on WAAM. First step studied only a single layer of material deposited on the substrate, observing their effects on the shape and quality of the bead. In the second stage, WAAM multiple layers were deposited with a focus to study the walls formed.

All weld beads were deposited with a pre heating and interpass temperature control of 100°C always using the same direction, as shown in Figure 1. To measure the interpass temperature, a type K thermocouple and infrared thermometer Minipa 850MT was used at the basis of the weld bead. To help achieve this objective, a 12V cooler was used, producing forced convection between one pass and another. During the welding process, this device remained off. Figure 1 shows the details of the operation, along with the fixation system used.

2.3. Methodology and parameters selection

The methodology used for the selection of the parameters used was a variation of the factorial statistical method, called Central Composite Circunscrit (CCC), in which low, medium and high level values of the variables to be studied are determined. These values are arranged in a cube, in which its axes are the variables to be merged and its vertices are the parameter values already merged. If the number of variables studied is greater than three, levels are created on the axes so that the intersection of all variables is possible. The CCC methodology provides six star-points. The star-points are outside the cube, at a certain distance from the center (identified by the Greek letter alpha "α"). This distance is the radius of the sphere circumscribed in the cube, establishing higher extremes for the low and high configurations for the studied factors, extrapolating the low and high values determined previously. The CCC design of experiment, therefore, can study not just the values inside the low and high values inside the cube, but also higher and lower parameters values. Figure 2 illustrates the CCC experiment design methodology.
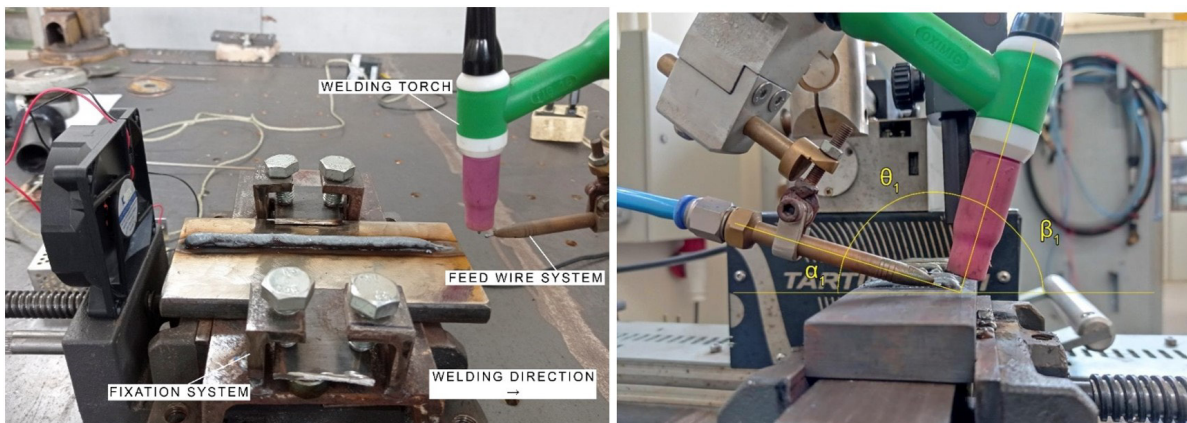

Figure 1. Interpass-cooling set-up used to control the interpass temperature.
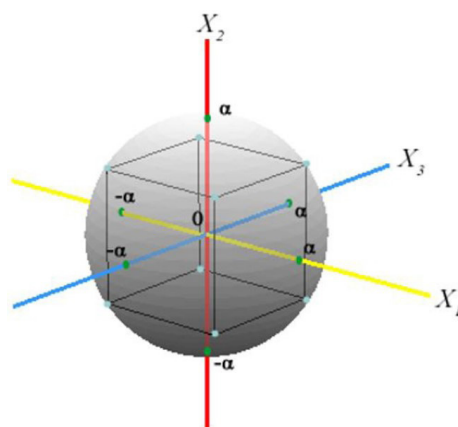

Figure 2. Graphical representation of the experiment design – CCC.

In this work, the following variables were studied: peak current (Cp), base current (Cb), wire feed speed at peak current (Vap), wire feed speed at base current (Vab) and welding (Vs). The definition of low, medium and high levels of the initial parameters is shown in Table 2. To select such levels, a preliminary study was carried out guided by the literature.

Table 2. Low, Medium and High Level (Cubic Points) of the variable parameters used in this work.

Level	C_p [A]	C_b [A]	Va_p [m/min]	Va_b [m/min]	Vs [cm/min]
Low	175	75	2.2	1.1	15
Medium	200	100	2.4	1.2	20
High	225	125	2.6	1.3	25

Once the limit values of the variables are determined, the calculation and distribution of their combination is obtained using Minitab® software. In Table 3 it is possible to observed the star points of the CCC methodology, parameters #7, #9, #16, #21, #25, #28, #29, #37, #39 and #45, these points increase the research envelope of the study.

Table 3. Experiment parameters for using the CCC methodology.

Level	C_p [A]	C_b [A]	Va_p [m/min]	Va_b [m/min]	Vs [cm/min]	Level	C_p [A]	C_b [A]	Va_p [m/min]	Va_b [m/min]	Vs [cm/min]
1	175	125	2.2	1.3	25	27	225	125	2.6	1.1	15
2	175	75	2.6	1.3	15	28	200	100	2.4	1	20
3	200	100	2.4	1.2	20	29	200	40	2.4	1.2	20
4	175	75	2.2	1.1	15	30	200	100	2.4	1.2	20
5	175	75	2.2	1.3	15	31	175	75	2.6	1.1	25
6	225	125	2.2	1.1	25	32	225	125	2.6	1.3	25
7	200	100	2.4	1.2	8	33	225	75	2.2	1.1	25
8	175	75	2.2	1.3	25	34	200	100	2.4	1.2	20
9	200	100	1.9	1.2	20	35	225	75	2.6	1.1	15
10	175	125	2.6	1.3	25	36	175	75	2.6	1.1	15
11	175	125	2.6	1.3	15	37	140	100	2.4	1.2	20
12	200	100	2.4	1.2	20	38	175	125	2.6	1.1	25
13	225	125	2.2	1.3	25	39	200	100	2.9	1.2	20
14	225	75	2.2	1.3	25	40	175	75	2.2	1.1	25
15	225	125	2.6	1.1	25	41	175	75	2.6	1.3	25
16	260	100	2.4	1.2	20	42	225	75	2.2	1.1	15
17	200	100	2.4	1.2	20	43	225	125	2.6	1.3	15
18	200	100	2.4	1.2	20	44	225	75	2.2	1.3	15
19	200	100	2.4	1.2	20	45	200	100	2.4	1.2	32
20	175	125	2.6	1.1	15	46	200	100	2.4	1.2	20
21	200	100	2.4	1.43	20	47	225	75	2.6	1.3	25
22	175	125	2.2	1.3	15	48	225	75	2.6	1.1	25
23	175	125	2.2	1.1	15	49	225	125	2.2	1.1	15
24	175	125	2.2	1.1	25	50	200	100	2.4	1.2	20
25	200	160	2.4	1.2	20	51	225	75	2.6	1.3	15
26	200	100	2.4	1.2	20	52	225	125	2.2	1.3	15

To avoid systematic errors, the initial set of experiments was arranged in random order as shown in Table 3.

2.4. Ideal parameters definition

After the feasibility analysis of the set of parameters, based on the analysis of the bead continuity, the cross section of the weld beads deposited was evaluated using the parameters listed in Table 4, Aspects of reinforcement geometry, dilution, wettability and inscribed area were measured . These measurements were performed using a ZEISS® Axio stereoscopic microscope, using the ZEISS® AxioVision SE64 Rel. 4.9.1 software.

To evaluate the reinforcement geometry of the parameters, the height (H) and width (L) of the weld bead reinforcement were measured, seeking values for the Bead Area/Area ratio close to 1 (one), showing that the Welding bead reinforcement is a square. The evaluation of the dilution of the weld bead in the base metal was another evaluated factor, for this purpose the reinforcement area above the Base Metal and the melted area of the Base Metal were measured, determining the diluted percentage of the base metal. The lowest dilution values were sought.

To assess wettability, the angle (θ) formed between the base metal and the tangent of the weld bead reinforcement was measured. Values as close as possible to 90º were sought. To check whether the weld bead has conditions that can be used to build a structure using WAAM, a reference of filled area within the maximum cross-sectional area that the bead has was used. The area of the bead reinforcement was measured and divided by the area between base and height. After measuring AREA 1 (larger area) and AREA 2 (smaller area, inscribed in AREA 1), the ratio between AREA 2 and AREA 1 was calculated. If this ratio is equal to 1 (one), it means that all the possible area was filled, something of excellence for additive manufacturing processes. Although this relationship is impossible due to the manufacturing process used, values as close as possible to 1 (one) are sought.

2.5. WAAM manufaturing samples parameters for the second stage

After carrying out the study of the parameters, based on the initial research defined in section 2.4, the welding parameters used in the preparation of the samples built layer by layer were defined, observed in Table 4.

Table 4. Parameters used in the pulsed GTAW process.

Process Parameters	Value
Peak current	200 A
Base Current	100 A
Welding Tension (average)	14 V
Welding speed	20 cm/min
Peak of frequency	10 Hz
Base of frequency	10 Hz
Polarity	CC -
Shielding gas	Argon; 12 L/min
Nozzle diameter	10 mm
Electrode (W+2%ThO2)	$\emptyset$ 2.4 mm
Electrode tip angle	60º
Arc length	3 mm
Wire feed rate (VP50IM)	$\emptyset$ 1.2 mm
Wire feed rate (peak)	2.9 m/min
Wire feed rate (base)	1.2 m/min
Wire incidence angle (α1)	15º
Torch incidence angle (β1)	75º
Angle between torch and wire (θ1)	90º

2.6. WAAM hardness mapping

The purpose of the Vickers micropenetration hardness test is, in addition to measuring the weld bead hardness, to measure the behavior of the HAZ. For this purpose, the Shimadzu® HMV-G20 Series Microscale Durometer was used. The test was carried out in acbeadance with ASTM E384-11 [26], for Vickers hardness with a preload of 300 gf. Three series of measurements were performed, with a spacing of 1mm between each measurement to create the hardness map along the welded structure.

2.7. Tensile properties measurement of the WAAM samples

The EMIC® Line DL-10000 machine with a capacity of up to 100 kN was used, applying a variation of the ASTM E 8M-04 standard [27]. Two series of specimens were made, one specimen removed from the cross section (body A) of the deposited weld beads; another removed in the longitudinal section (body B), shown schematically in Figure 3.
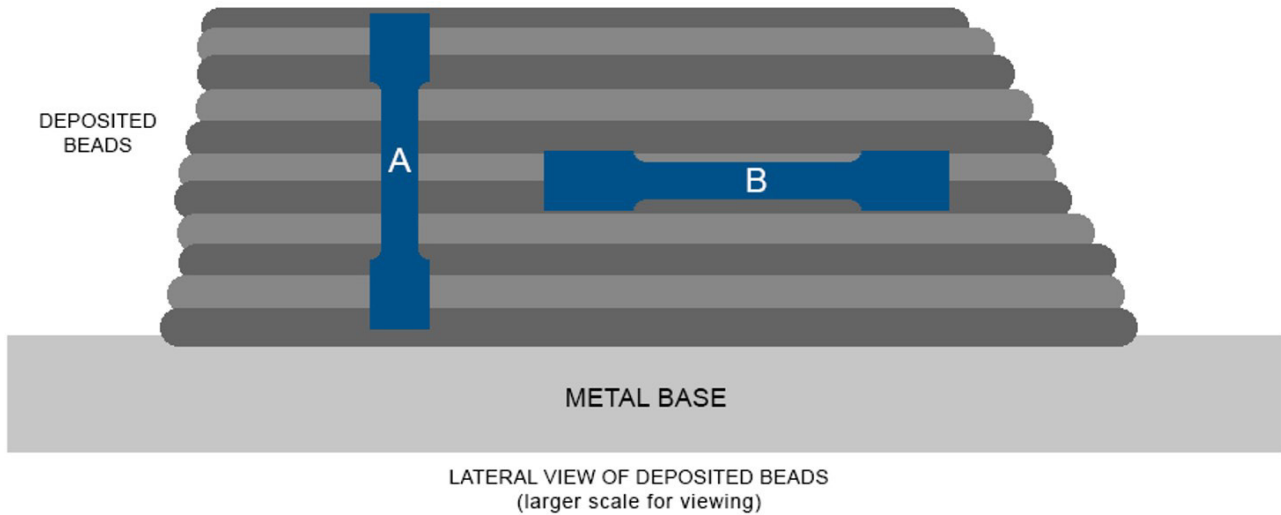
Figure 3. Schematic drawn of the specimens for tensile testing (A) Transversal (B) Longitudinal.

3. Results and Discussion

3.1. Parameters influence, first stage

The weld beads deposited with the parameters presented in Table 3 are visualized in Figure 4. It is possible to identify the parameters that present a better visual appearance, either due a continuous weld bead and geometry consistency. Parameters #7, #29, #31, #37, #40 and #41 were discarded due not to form a continuous weld bead. Especially for weld bead number #7, the ratio between deposited energy and welding speed was not possible to start the electric arc, as observed in Dinovitzer et al. [9].
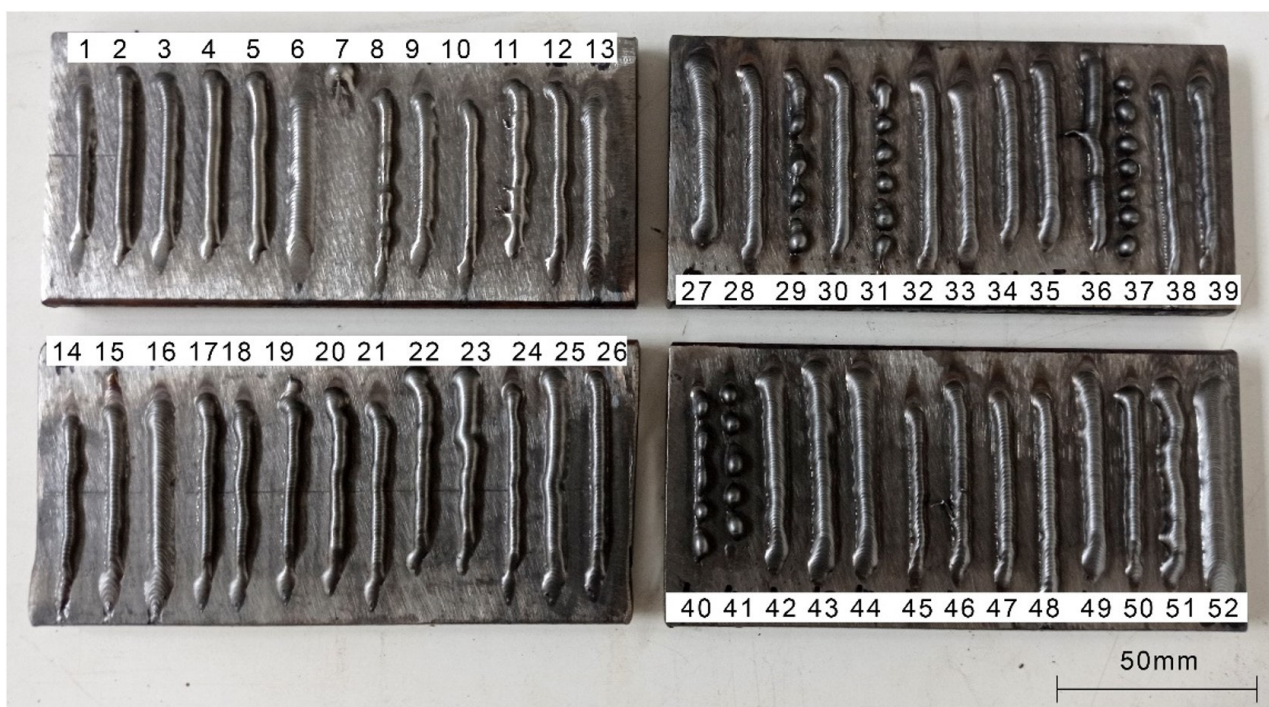

Figure 4. Results of making the weld beads for the 52 experiments described in the Table 3.

After this initial selection, the samples were cut, allowing the observation of their cross-section. The base (b), height (h) and ratio (r) values between the height and the base are shown in Table 5. An example of the measurement carried out to obtain the dimensions shown in Table 5 can be seen in Figure 5. The 4.14 mm measurement corresponds to values for the width of the bead (b), the 1.94 mm measurement corresponds to the reinforcement of the bead (h) and the measurement of 5.84 mm^2 corresponds to the area occupied by the reinforcement of the bead, in its transversal section.

Table 5. Initial study geometry measurements.

| Level	b [mm]	h [mm]	r [mm/mm]	Level	b [mm]	h [mm]	r [mm/mm]	Level	b [mm]	h [mm]	r [mm/mm]
1	4.14	1.94	0.469	19	3.56	2.95	0.829	37	-	-	-
2	4.65	3.23	0.695	20	4.72	3.6	0.763	38	3.03	2.86	0.944
3	4.81	2.43	0.505	21	4.73	2.83	0.598	39	4.03	2.68	0.665
4	4.66	2.67	0.573	22	4.92	2.92	0.593	40	-	-	-
5	4.6	2.84	0.617	23	4.56	2.81	0.616	41	-	-	-
6	7.32	1.37	0.187	24	4.01	2.15	0.536	42	4.9	2.64	0.539
7	-	-	-	25	6.02	2.21	0.367	43	5.34	2.73	0.511
8	3.89	2.66	0.684	26	4.23	2.52	0.596	44	6.12	2.5	0.408
9	5.3	1.98	0.374	27	6.72	2.31	0.344	45	3.4	2.06	0.606
10	4.17	2.24	0.537	28	4.85	2.22	0.458	46	4.71	2.31	0.490
11	4.82	2.86	0.593	29	-	-	-	47	4.62	2.12	0.459
12	4.67	2.41	0.516	30	4.88	2.51	0.514	48	4.4	2.111	0.480
13	3.99	2.4	0.602	31	-	-	-	49	5.93	2.48	0.418
14	3.99	2.4	0.602	32	4.31	2.33	0.541	50	3.83	2.63	0.687
15	4.61	2.28	0.495	33	5.47	1.66	0.303	51	5.16	3.19	0.618
16	6.3	1.98	0.314	34	4.36	2.72	0.624	52	8.96	2.03	0.227
17	4.16	2.54	0.611	35	5.37	2.92	0.544				
18	4.03	2.66	0.660	36	3.65	2.79	0.764				
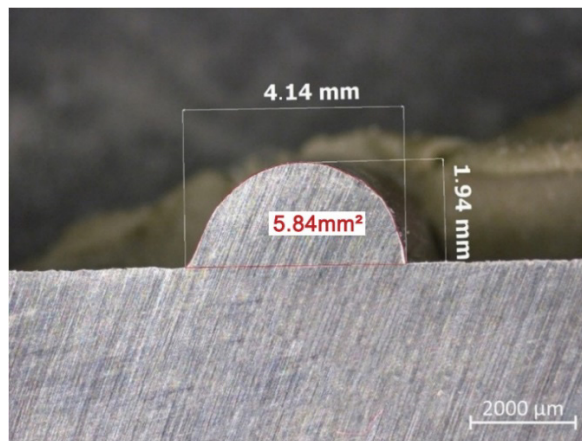
Figure 5. Geometric analysis: Cross section parameter 01.

During the geometry analysis, it was possible to analyze some defects in some parameters that make it impossible to continue in the study, such as porosity and/or lack of fusion, as observed in Figure 6. Therefore, parameters #02, #08, #20, #21, #22, #30, #35, #36, #45, #48 and #49 were discarded.
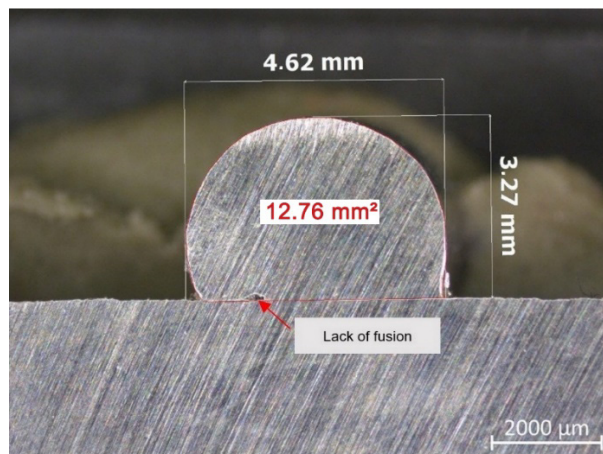

Figure 6. Geometric analysis: Cross section parameter 02.

Continuing the analysis of the geometry of the cross-section of the parameters, the samples that presented a ratio between reinforcement heigth and width (r) below 0.55 were discarded, due to the lower efficiency of building a wall using the WAAM technique. The "r" value equal to 1 means that the cross section of the weld reinforcement has the same height and base value, being ideal for the formation of an additive geometry. Values below 0.5 mean that the height is less than twice the width, forming a ratio rectangle not contributing to the formation of a layer-to-layer geometry.

Thus, after an analysis of the data as a whole, ratio values above 0.55 were chosen in order to apply one more filter to the samples. The area of the bead reinforcement envelope (area per height) and the effective area of the bead in this envelope were analyzed in the cross section of the solder bead, as shown in Figure 7. This measurement methodology was followed for all samples. The results of the areas, as well as their calculated ratios are observed in Table 6.
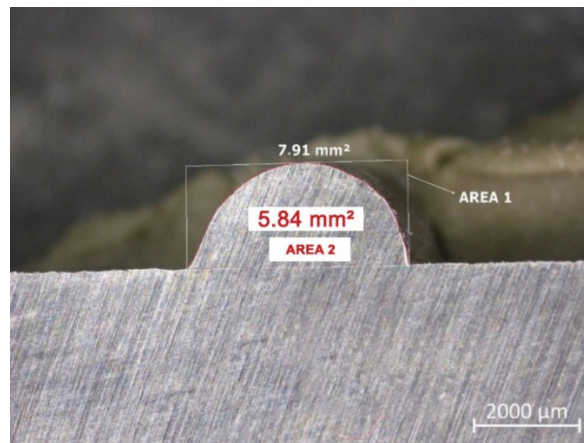

Figure 7. Area analysis: Cross section parameter 01.

Table 6. List of registered areas of reinforcement of the weld beads.

NÍVEL	AREA1 [mm]	AREA2 [mm]	r= AREA2/ AREA1	NÍVEL	AREA1 [mm]	AREA2 [mm]	r= AREA2/ AREA1	NÍVEL	AREA1 [mm]	AREA2 [mm]	r= AREA2/ AREA1
1	-	-	-	19	8.89	10.46	0.85	37	-	-	-
2	-	-	-	20	-	-	-	38	7.26	8.54	0.85
3	8.83	11.75	0.75	21	-	-	-	39	9.09	10.77	0.84
4	10.32	12.59	0.82	22	-	-	-	40	-	-	-
5	10.55	13.03	0.81	23	10.18	12.81	0.79	41	-	-	-
6	-	-	-	24	6.58	8.61	0.76	42	10.01	12.82	0.78
7	-	-	-	25	-	-	-	43	10.91	14.52	0.75
8	-	-	-	26	8.55	10.63	0.80	44	-	-	-
9	-	-	-	27	-	-	-	45	-	-	-
10	7.24	9.25	0.78	28	-	-	-	46	-	-	-
11	11.18	13.68	0.82	29	-	-	-	47	-	-	-
12	8.74	11.36	0.77	30	-	-	-	48	-	-	-
13	7.14	9.41	0.76	31	-	-	-	49	-	-	-
14	7.14	9.41	0.76	32	-	-	-	50	8.12	10.06	0.81
15	-	-	-	33	-	-	-	51	12.79	16.15	0.79
16	-	-	-	34	9.45	11.84	0.80	52	-	-	-
17	8.31	10.51	0.79	35	-	-	-				
18	8.55	10.73	0.80	36	-	-	-				

For the application of the area filter, samples with a ratio "r" between AREA 2 and AREA 1 greater than 0.80 were chosen. Based on the results obtained, it was possible to select the better parameters levels are the parameters #04, #19, #38 and #39. For the wettability analysis of the last four levels, the angles of the cross-section of the selected samples were measured. The measurements are explained in Figure 8. Wetting angle was also used to evaluate the optimal parameters in Dinovitzer et al. [9] using GTAW process, in Baffa et al. [28] using Gas Metal Arc Welding (GMAW), and in Oliari et al. [29] which used wire-based Laser metal deposition. The deposition of weld beads with wetting angle lower than 90° would induce lower surface quality deposition and voids between the deposited layers, reducing the overall quality of the WAAM deposited wall. In this way, the parameters of levels 38 and 39 become candidates for choosing the ideal parameter. Despite on the differences between the additive manufacturing processes, the deposition of weld beads with wetting angle higher than 90 degrees reduce the chance of defects during the deposition.
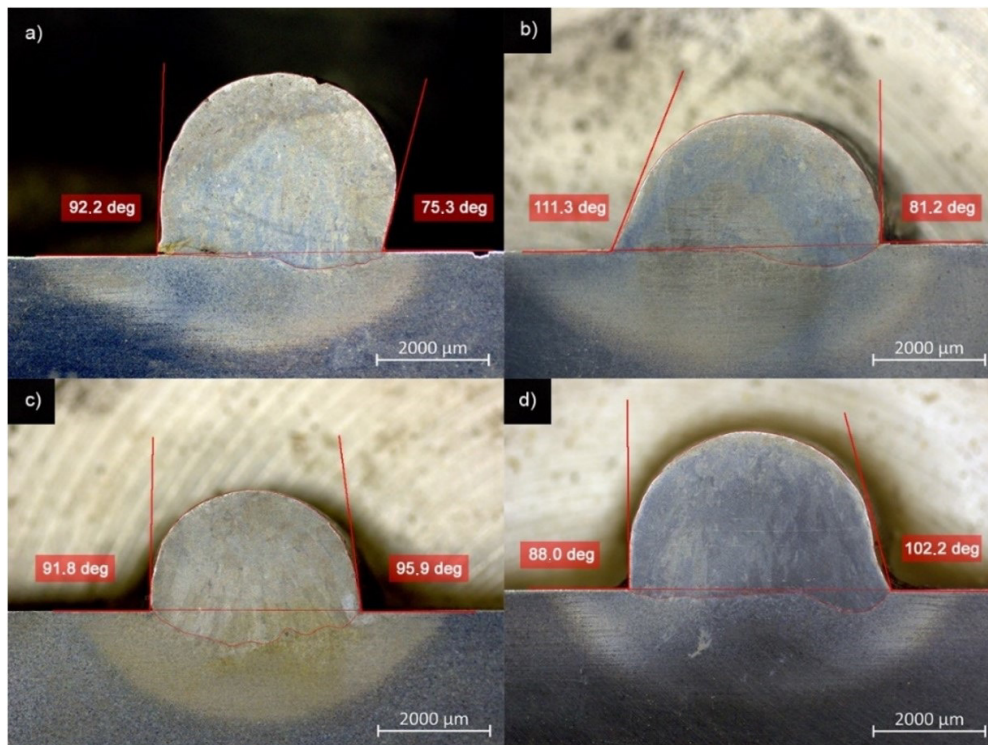
Figure 8. Weld beads of the samples from the following levels: (a) 4; (b) 19; (c) 38; (d) 39.

Finally, the last analysis in order to determine the ideal parameter for the study was the dilution. The dilution of the reinforcement in the substrate is essential to quantify the amount of energy transferred to the substrate. In additive manufacturing, low dilution values are important, since for stacked structures the minimum transfer of thermal energy is sought to avoid interference from one layer to the other [22], Another important aspect is the surface waviness decreases with the heat input increase, due to the ability of the molten metal to provide sufficient energy to support material flow [30]. Figure 9 shows the area values related to the dilution of the studied levels.
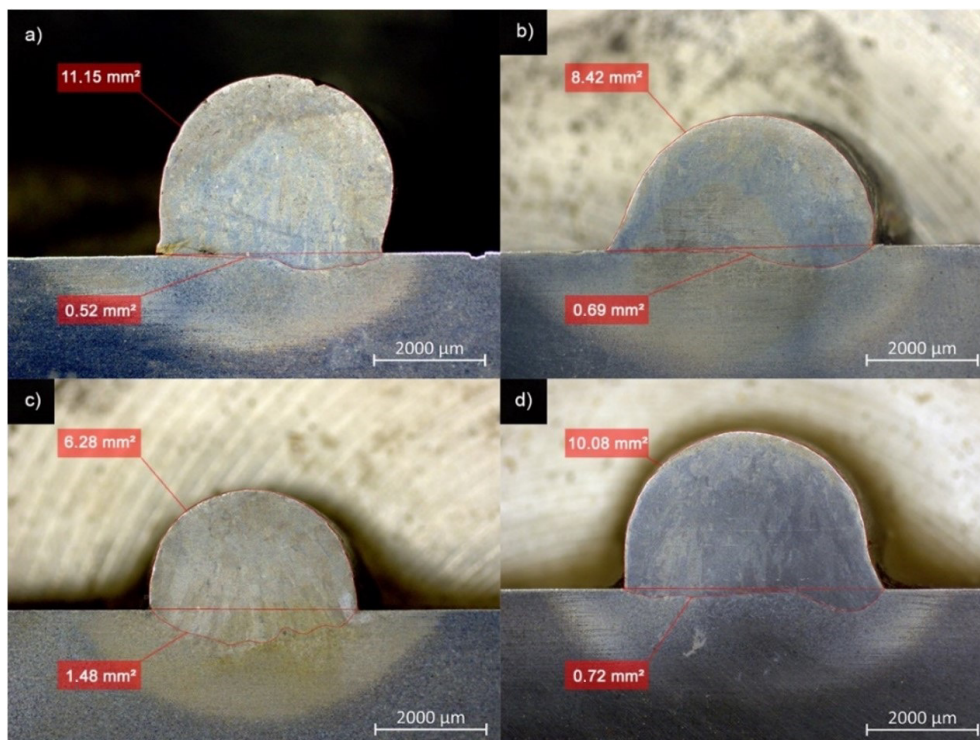

Figure 9. Dilution of the samples, levels: (a) #04; (b) #19; (c) #38; (d) #39.

The calculated dilution values were: #04 = 4.3%; #19 = 7.5%; #38 = 19.1%; #39 = 6.6%. The level 04 sample, despite having low dilution values, was discarded for showing evidence of lack of melting of the base metal. This lack of melting can subsequently lead to porosity and possibly of discontinuity during the deposition of the layers. In Lin et al. [30] the authors used a process window for WAAM using GMAW process between 5% to 20% of dilution. In this work the authors considered an ideal dilution between 10% to 20%, and a relation between height/width from 0.25 to 0.36, however the WAAM was planned to deposit wider areas, not a thin wall, as the present research.

The qualitative relationship between welding speed (Vs) and wire feed (Va) is directly proportional to the stability of the arc, making it possible to change the microstructure and mechanical properties just by varying the welding speed and maintaining the same amount of energy [11], which would change the rate of deposited energy. The literature [9,21] argues that the effective width of a wall manufactured by WAAM increases with decreasing welding speed and increasing wire feed speed. By controlling the torch speed and wire feed speed, the columnar grains are changed to fine equiaxed grains. Welding speed and current inversely contribute to heat input. Increasing the displacement speed or decreasing the current causes a decrease in the depth of fusion and an increase in the lateral roughness of the deposited layer.

From the first experimental stage, the level 39 parameter was chosen, with the following parameter variables:

• C_p = 200 A

• C_b = 100 A

• Va_p = 2.9 cm/min

• Va_b = 1.2 cm/min

• Vs = 20 cm/min

3.2. WAAM microstructure and properties, second stage

The samples did not show the presence of cracks or larger porosities visible to the naked eye and after liquid penetrating test, following the expected parallelism and orthogonality as can be seen in Figure 10 (larger sample, for the transverse specimens) and in Figure 11 (smaller sample, for the longitudinal specimens).

Figure 10. Wall deposited for transversal tensile testing samples.

It is possible to observe a considerable decay at the end of the piling weld beads. This event is related to the fact that the stacking welding occurs in only one direction, combined with an early interruption when executing the 5th pass, which was replicated for the others. To avoid this event, the literature [31] recommends a previous study of the torch path, performing the welding of passes in opposite directions. In another study, Ti6Al4V deposited with Pulsed PAW showed a slighter collapse of the end of the thin-walled structure compared to GTAW [10]. The location of the samples for cross-sectional analysis and tensile testing are shown in Figure 12 and Figure 13.

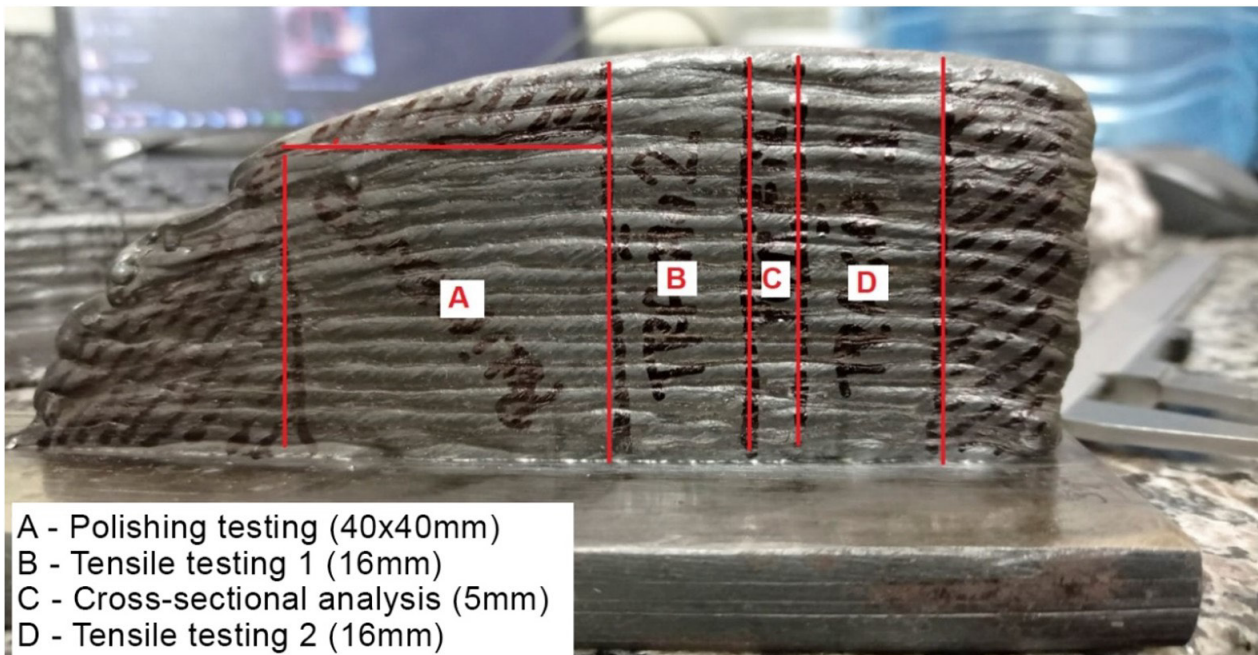**Figure 11.** Wall deposited for longitudinal tensile testing samples.

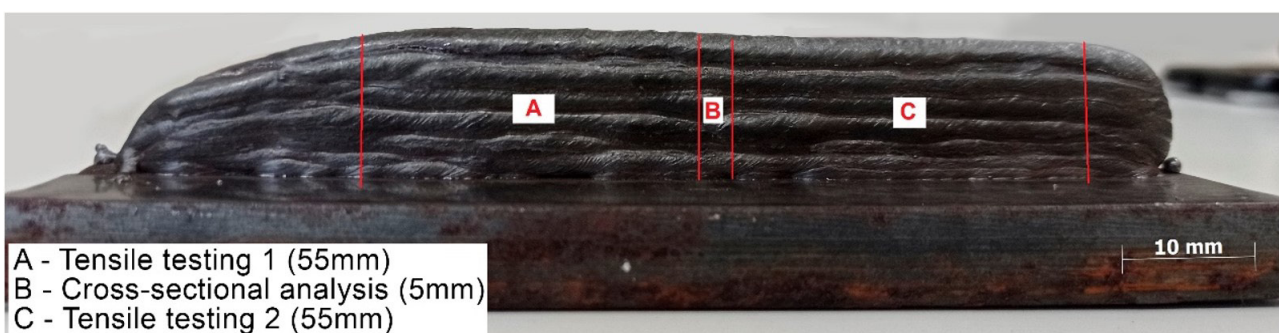**Figure 12.** Schematic drawn for transversal sampling.

Figure 13. Schematic drawn for longitudinal sampling.

The cross-sectional analysis is available in Figure 14. In this image, it is possible to observe the total size of the weld beads, as well as the microstructure along the stack. It is possible to observe ferrite and cementite both in the beginning and in the middle of the structure. At its top, in the final weld beads, cementite is more easily visualized. The formation of thicker cementite may be related to the tempering by subsequent deposition layer, since this last bead is cooled more slowly, in addition to not suffer another thermal cycling by other deposition layer. From the successive layers deposited, new zones with different microstructures are formed due to the heating and cooling of the previously deposited material. These mechanisms are common in the additive manufacturing of metallic parts, where the energy transferred by the power source and cooling influence the final microstructure, being retained in non-heat-treated WAAM deposits.

No internal defects (cracks, porosity, lack of fusion) were observed in the manufactured walls, based on the macrographs analyzes carried out. From the heterogeneity observed in the macrostructure, it was possible to notice three zones with distinct microstructures, these zones would be refined grains, partially refined grains and coarse grain zones, common regions found in the heat-affected zone in multi-pass welded joints [18,20,28,32].
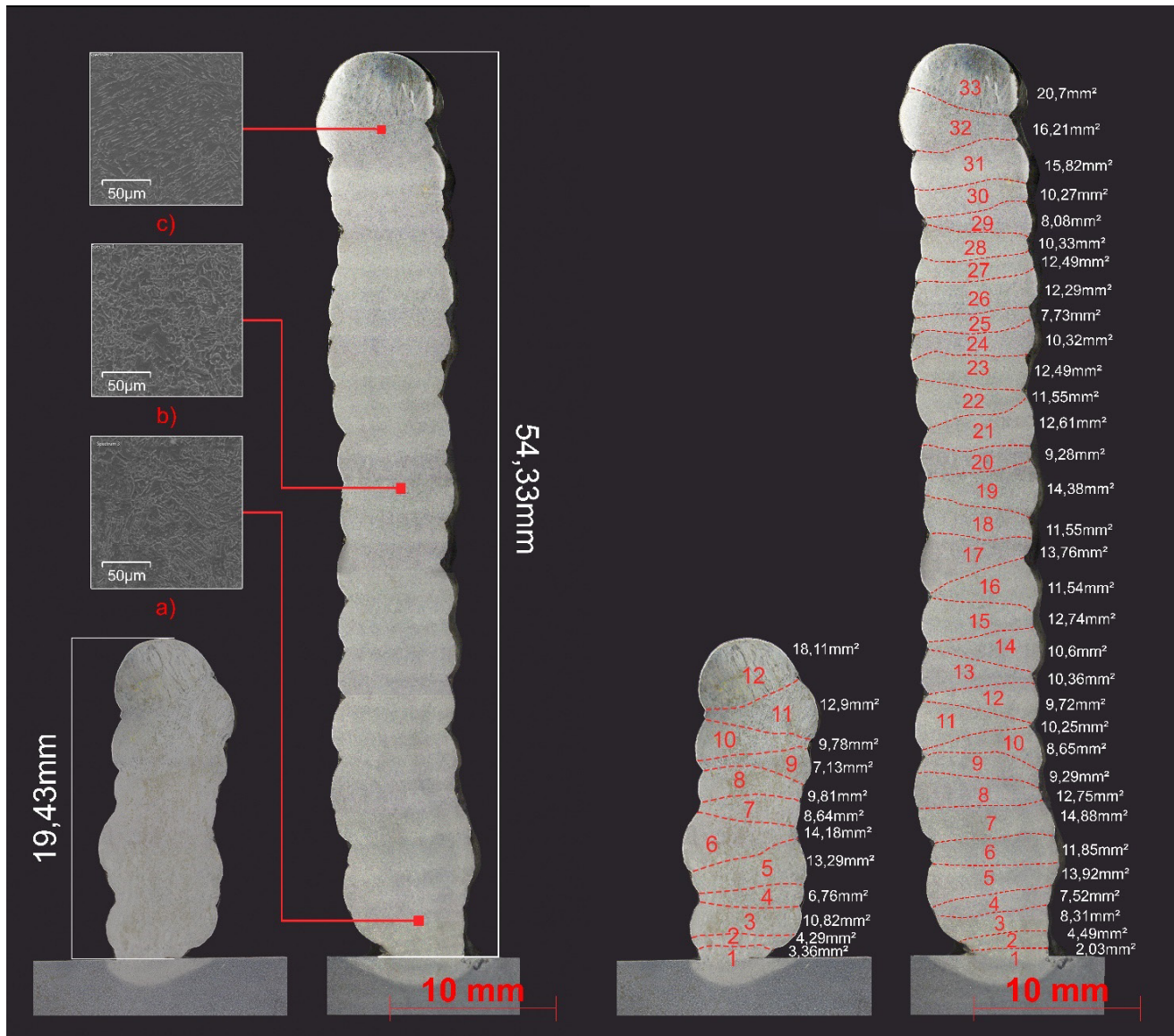

Figure 14. Cross-section of layer-by-layer welding. (a) Microstructure of the beginning of the structure (2nd layer); (b) Microstructure of the middle of the structure (19th layer); (c) Microstructure of the top of the structure; (d) Welding dilution layer by layer (32th layer).

It can be seen that the first weld beads tend to be narrower and taller than the others, Figure 15, both in the larger sample and in the smaller sample, because the heat distribution is less localized. This bead size pattern is also visualized in the literature [10,18,33], as a result of the thermal influence of the adjacent layer on the previous layer, where the mixture of welded materials and microstructures are remelted. According to [10] in the first deposition layers, heat is dissipated into the substrate through conduction, resulting in a higher cooling rate, with a narrow deposited layers. As building height increases, the heat transfer mode is modified to include a greater proportion of convective and radiative modes. This limits effective heat dissipation, resulting in a slower cooling rate of the melt, increasing the width of subsequent layers. As additional layers are deposited the wall achieves stability. Thus, geometric inaccuracies are often produced in the first layers by WAAM.

The area values of the diluted weld beads in the cross-sectional and longitudinal samples, previously illustrated in Figure 15, are distributed in Table 7. To facilitate the analysis, a percentage of the area of the diluted bead and accumulated area was also added, for a better visualization of the total stacking.

Table 7. Diluted bead area values in stacked samples.

Bead N°	TRANSVERSAL SAMPLE			LONGITUDINAL SAMPLE		
	Area [mm²]	Area [%]	Total Area [%]	Area [mm²]	Area [%]	Total Area [%]
33	20.7	6%	100%	-	-	-
32	16.21	4%	94%	-	-	-
31	15.82	4%	90%	-	-	-
30	10.27	3%	86%	-	-	-
29	8.08	2%	83%	-	-	-
28	10.33	3%	81%	-	-	-
27	8.89	2%	78%	-	-	-
26	12.29	3%	75%	-	-	-
25	7.73	2%	72%	-	-	-
24	10.33	3%	70%	-	-	-
23	12.49	3%	67%	-	-	-
22	11.55	3%	64%	-	-	-
21	12.61	3%	60%	-	-	-
20	9.29	3%	57%	-	-	-
19	14.38	4%	54%	-	-	-
18	11.55	3%	50%	-	-	-
17	13.76	4%	47%	-	-	-
16	11.54	3%	44%	-	-	-
15	12.74	3%	40%	-	-	-
14	10.6	3%	37%	-	-	-
13	10.36	3%	34%	-	-	-
12	9.72	3%	31%	18.11	15%	100%
11	10.25	3%	28%	12.9	11%	85%
10	8.65	2%	26%	9.78	8%	74%
9	9.29	3%	23%	7.13	6%	66%
8	12.75	3%	21%	9.81	8%	60%
7	14.88	4%	17%	8.64	7%	52%
6	11.85	3%	13%	14.18	12%	44%
5	13.92	4%	10%	13.29	11%	32%
4	7.52	2%	6%	6.76	6%	21%
3	8.31	2%	4%	10.82	9%	16%
2	4.49	1%	2%	4.29	4%	6%
1	2.03	1%	1%	3.36	3%	3%

When analyzing Table 7, it is observed that the first weld beads promoted a lower contribution with the total height of the wall, as described previously. The dilution of the chemical elements along the WAAM thin wall constructed can be observed in Table 8. Regions A, B and C, Figure 14, correspond respectively to the beginning (weld bead number 3), middle (weld bead number 19) and top regions (weld bead number 32) of the stacked structure.

Table 8. Dilution of chemical elements during stacking.

	Fe [Wt%]	Ni [Wt%]	Mn [Wt%]	Si [Wt%]	Cr [Wt%]	Mo [Wt%]
Substrate	98.3	-	1.7	-	-	-
A Area	95.4	2.1	1.8	0.1	0.3	-
B Area	95.1	2.4	1.4	0.3	0.3	0.4
C area	95.1	2.5	1.5	0.3	0.3	0.4

The data presented in Table 8 corroborate that at the beginning of the WAAM process, the chemical elements showed a stronger influence of the base metal dilution. This transient regime at the beginning of the process causes a properties influence from the beginning and end of the sample, not only in the dilution, but also in the mechanical properties as visualized in the Microhardness mapping. The high intrinsic heat input of the welding process leads to inevitable heat treatments during the process [34]. In WAAM, due to the large amount of thermal cycles and remelting of the previous layers by the adjacent layers causes an important microstructural changes, for example, the last weld beads in both samples showed higher microhardness values indicating a recristalization process during the WAAM wall construction by subsequent deposited layers. As described in

Duan et al. [10] the use of pulsed arc contribute with an increase of the cooling rate and consequently with the grain refining process and better properties than conventional deposition process without the use of pulsed arc.

Figure 15 shows the Vickers microhardness (HV) map of the welded samples layer by layer, where the abscissa axis represents the length of the specimen and the coordinate axis the microhardness value. The microhardness values observed in present research is similar than obtained in Preciado and Bohorquez [35] the research conduced with AISI P20 and VP50IM deposited with GTAW process to repair polymer injection molds.
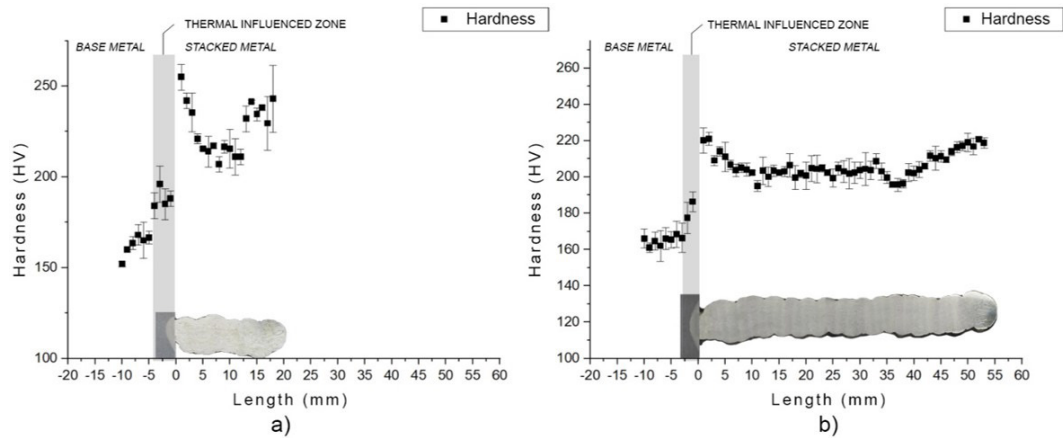

Figure 15. Hardness mapping: (a) Sample 1 (transverse); (b) Sample 2 (longitudinal).

The hardness of welded samples may be related to the amount of energy deposited during the welding process, in addition to the thermal treatment induced during the deposition of this energy. It is possible to observe in Figure 15 a decrease in the hardness measured in the central region of the specimen by an average of 9%. This hardness decay starts from 5mm, from the 3rd deposited bead and remained constant until the last two deposited weld beads, where the hardness increases again. It can be observed that the way the stacking process develop, there is a stabilization of these, collaborating for a stabilization of the stacking hardness properties. This decrease in hardness from the base metal surface to the wall, can be related to the lower cooling rate observed during the wall height increase, as observed previously in WAAM studies and laser-arc hybrid process [10,14,18]. The accumulation of heat affects the microhardness of the weld beads deposited outside the steady state [33] that is, at the beginning and end of the weld, where the cooling rate of the weld beads changes.

Table 9 shows the results of the tensile tests, where A1 and A2 are specimens in the longitudinal direction of the welding direction and B1 and B2 are specimens in the transverse direction of the welding direction.

Table 9. Uniaxial tensile test results.

	Yelding Stress [MPa]	Tensile Stress [MPa]	Area reduction [%]
A 1	633.25±32	642.5±32	39.1±2
A 2	562.75±28	655.9±34	37.2±2
B 1	529.80±29	638.8±31	34.8±2
B 2	514.14±26	634.1±31	38.0±2

Thus, by analyzing Table 9, the longitudinal specimens submitted to the tensile test showed a yield stress of up to 15% greater than the transverse specimens and an average area reduction of up to 5% less. The results observed in Table 9 showed similar results than [36] in 5Cr5Mov steel. In WAAM processes it is possible to observe that the thermal cycles occurred during welding has a direct influence on the result of tensile tests of samples. In order to reduce the accumulation of heat, which decreased with prolonged cooling improve such properties because the remelted cellular crystals between the layers are relatively short. However, increasing the waiting time for cooling between layers generates more impurities and oxides between layers, which can be detrimental to the results of transverse tensile tests compared to longitudinal ones [34].

4. Conclusions

A high sensitivity of the pulsed GTAW process parameters for WAAM was observed, in which a slight change in the torch angle or wire feeding change the final result. When carrying out an experiment of this nature using such machines and processes, it is recommended to manufacture angle and stop templates, in order to eliminate as much as possible gaps and vibrations in the feeding of wire, torch and base metal, in addition to an execution of Systematic and methodical experiment to guarantee the best possible results.

The selection of the parameter for the study showed good results, validated by the manufactured geometry, showing that the analysis of parameters such as dilution, wettability and reinforcement geometry are important factors when selecting the parameter Cp=200A, Cb=100A, Vap=2.9cm /min, Vab=1.2cm/min and Vs=20cm/min for making a structure using MA.

The longitudinal specimens submitted to the tensile test showed an average yield stress of 598Mpa in the longitudinal direction of the weld bead deposition and 522 in the transverse direction. That is, there was an increase in the yield stress of up to 15% in relation to the direction of deposition of the stacked boulders. Thus, when determining the path of the torch in the manufacture of an additive tool, it is important to consider the direction in which the stacking is made, as it is influenced by the yield stress of the final part. The area reduction values presented an average of 37% of the initial area, with a variation of 5% between the tests in the transverse and longitudinal direction of stacking, showing a slightly greater ductility in the longitudinal direction of the weld beads.

Hardness mapping along the specimen showed lower hardness values in the central sections of the stack, as well as higher hardness values at the ends, reaching up to 9% of discordance. This fact is related to the tempering intrinsic to the layer-by-layer welding process, due to the amount of energy transferred to the material.

Authors' contributions

PHT: He completed his Master's thesis, which provided the basis for the article. He provided support from research planning, data collection, laboratory analysis and writing of the article. ASFF: Experimental data collection and text writing and review. RNV: Co-advisor of the work, he supported the planning of the work and the collection of field data. AGMP: Work advisor, supported in the study planning, field data collection, laboratory analysis and writing of the article.

References

[1] Thompson SM, Bian L, Shamsaei N, Yadollahi A. An overview of Direct Laser Deposition for additive manufacturing; Part I: transport phenomena, modeling and diagnostics. Additive Manufacturing. 2015;8:36-62. http://dx.doi.org/10.1016/j.addma.2015.07.001.

[2] Shamsaei N, Yadollahi A, Bian L, Thompson SM. An overview of Direct Laser Deposition for additive manufacturing; Part II: mechanical behavior, process parameter optimization and control. Additive Manufacturing. 2015;8:12-35. http://dx.doi.org/10.1016/j.addma.2015.07.002.

[3] Almeida AMD. Principais barreiras de implementação de manufatura aditiva no Brasil [dissertação de mestrado]. São Paulo: Universidade Nove de Julho; 2019.

[4] American Society for Testing and Materials. ASTM 52900:2015: standard terminology for additive manufacturing: general principles: terminology. West Conshohocken: ASTM; 2015. p. 1-9.

[5] Ding D, Pan Z, Cuiuri D, Li H. A multi-bead overlapping model for robotic wire and arc additive manufacturing (WAAM). Robotics and Computer-integrated Manufacturing. 2015;31:101-110. http://dx.doi.org/10.1016/j.rcim.2014.08.008.

[6] Rashid A. Additive manufacturing technologies. In: Chatti S, Laperrière L, Reinhart G, Tolio T, editors. CIRP encyclopedia of production engineering. Berlin: Springer; 2019. http://dx.doi.org/10.1007/978-3-662-53120-4_16866.

[7] Pei E, Bernaned A, Gu D, Klahn C, Monzón M, Petersen M, et al. Springer handbook of additive manufacturing. 1st ed. Cham: Springer; 2023.. http://dx.doi.org/10.1007/978-3-031-20752-5.

[8] Huang Y, Yang L, Xin Q. Novel geometrical model and design mechanical parameters for CMT-WAAM stainless steel. Journal of Constructional Steel Research. 2023;210:108071. http://dx.doi.org/10.1016/j.jcsr.2023.108071.

[9] Dinovitzer M, Chen X, Laliberte J, Huang X, Frei H. Effect of wire and arc additive manufacturing (WAAM) process parameters on bead geometry and microstructure. Additive Manufacturing. 2019;26:138-146. http://dx.doi.org/10.1016/j.addma.2018.12.013.

[10] Duan X, Li Q, Xie W, Yang X. Wire arc metal additive manufacturing using pulsed arc plasma (PAP-WAAM) for effective heat management. Journal of Materials Processing Technology. 2023;311:117806. http://dx.doi.org/10.1016/j.jmatprotec.2022.117806.

[11] Farias RM, Vilarinho LO. Computational simulations of metal additive manufacturing processes: an introductory review. Soldagem e Inspeção. 2022;27:1-9. http://dx.doi.org/10.1590/0104-9224/si27.03.

[12] Chen C, He H, Zhou J, Lian G, Huang X, Feng M. A profile transformation based recursive multi-bead overlapping model for robotic wire and arc additive manufacturing (WAAM). Journal of Manufacturing Processes. 2022;84:886-901. http://dx.doi.org/10.1016/j.jmapro.2022.10.042.

[13] Antonello MG, Bracarense AQ, Scheuer CJ, Freitas Daudt N. Effect of electromagnetic arc constriction applied in GTAW-based wire arc additive manufacturing on walls' geometry and microstructure. Journal of Manufacturing Processes. 2021;71:156-167. http://dx.doi.org/10.1016/j.jmapro.2021.09.015.

[14] Zhang Z, Wang Q, He Y, Wang X, Yuan S, Song G. Microstructure and properties of multi-layer and multi-bead parts of 316 stainless steel fabricated by laser-arc hybrid additive manufacturing. Optics & Laser Technology. 2024;168:109903. http://dx.doi.org/10.1016/j.optlastec.2023.109903.

[15] Pixner F, Buzolin R, Warchomicka F, Dománková M, Čaplovičová M, Riedlsperger F, et al. Influence of process and heat input on the microstructure and mechanical properties in wire arc additive manufacturing of hot work tool steels. Materials Science and Engineering A. 2023;888:145799. http://dx.doi.org/10.1016/j.msea.2023.145799.

[16] Nagasai BP, Malarvizhi S, Balasubramanian V. Effect of welding processes on mechanical and metallurgical characteristics of carbon steel cylindrical components made by wire arc additive manufacturing (WAAM) technique. CIRP Journal of Manufacturing Science and Technology. 2022;36:100-116. http://dx.doi.org/10.1016/j.cirpj.2021.11.005.

[17] Chen C, Sun G, Du W, Liu J, Zhang H. Effect of equivalent heat input on WAAM Al-Si alloy. International Journal of Mechanical Sciences. 2023;238:107831. http://dx.doi.org/10.1016/j.ijmecsci.2022.107831.

[18] Zhang J, Fan J, Xu J, Yang D, Peng Y, Wang K. The effect of heat input on the microstructure and mechanical properties of 18Ni 300 maraging steel fabricated by arc directed energy deposition. Materials Science and Engineering A. 2023;884:145545. http://dx.doi.org/10.1016/j.msea.2023.145545.

[19] Chen Z, Soh GS. Microstructure and mechanical properties of Wire Arc Additive Manufactured (WAAM) Inconel 718 parts via post heat treatments. Materials Today: Proceedings. 2022;70:567-573. http://dx.doi.org/10.1016/j.matpr.2022.09.592.

[20] Hackenhaar W, Mazzaferro JAE, Mazzaferro CCP, Grossi N, Campatelli G. Effects of different WAAM current deposition modes on the mechanical properties of AISI H13 tool steel. Welding in the World. 2022;66(11):2259-2269. http://dx.doi.org/10.1007/s40194-022-01342-0. PMid:37520498.

[21] Raut LP, Taiwade RV. Wire arc additive manufacturing: a comprehensive review and research directions. Journal of Materials Engineering and Performance. 2021;30(7):4768-4791. http://dx.doi.org/10.1007/s11665-021-05871-5.

[22] Rafieazad M, Nemani AV, Ghaffari M, Nasiri A. On microstructure and mechanical properties of a low-carbon low-alloy steel block fabricated by wire arc additive manufacturing. Journal of Materials Engineering and Performance. 2021;30(7):4937-4945. http://dx.doi.org/10.1007/s11665-021-05568-9.

[23] Su C, Chen X, Gao C, Wang Y. Effect of heat input on microstructure and mechanical properties of Al-Mg alloys fabricated by WAAM. Applied Surface Science. 2019;486:431-440. http://dx.doi.org/10.1016/j.apsusc.2019.04.255.

[24] Webster GA, Behvar A, Shakil SI, Ribble R, Chou K, Krishnamurthy A, et al. Wire arc additive manufactured AWS ER100S-G steel: very high cycle fatigue characterization. Engineering Failure Analysis. 2023;154:107721. http://dx.doi.org/10.1016/j.engfailanal.2023.107721.

[25] Wang X, Wang J, Gao Z, Xia DH, Hu W. Fabrication of graded surfacing layer for the repair of failed H13 mandrel using submerged arc welding technology. Journal of Materials Processing Technology. 2018;262:182-188. http://dx.doi.org/10.1016/j.jmatprotec.2018.06.040.

[26] American Society for Testing and Materials. ASTM E384-11: standard test method for knoop and vickers hardness of materials. West Conshohocken: ASTM; 2011.

[27] American Society for Testing and Materials. ASTM E8M-04: tension testing of metallic materials. West Conshohocken: ASTM; 2008.

[28] Baffa F, Venturini G, Campatelli G, Galvanetto E. Effect of stepover and torch tilting angle on a repair process using WAAM. Adv. Manuf. 2022;10(4):541-555. http://dx.doi.org/10.1007/s40436-022-00393-2.

[29] Oliari SH, D'Oliveira ASCM, Schulz M. Additive manufacturing of H11 with wire-based laser metal deposition. Soldagem e Inspeção. 2017;22(4):466-479. http://dx.doi.org/10.1590/0104-9224/si2204.06.

[30] Lin Z, Ya W, Subramanian VV, Goulas C, di Castri B, Hermans MJM, et al. Deposition of Stellite 6 alloy on steel substrates using wire and arc additive manufacturing. International Journal of Advanced Manufacturing Technology. 2020;111(1-2):411-426. http://dx.doi.org/10.1007/s00170-020-06116-w.

[31] Ding D, Pan Z, Cuiuri D, Li H. A tool-path generation strategy for wire and arc additive manufacturing. International Journal of Advanced Manufacturing Technology. 2014;73(1-4):173-183. http://dx.doi.org/10.1007/s00170-014-5808-5.

[32] Pereira HCB, Henke SL, D'Oliveira ASCM. IN625 multilayers characterization deposited by CMT. Soldagem e Inspeção. 2018;23:235-246. http://dx.doi.org/10.1590/0104-9224/si2302.10.

[33] Xu X, Mi G, Luo Y, Jiang P, Shao X, Wang C. Morphologies, microstructures, and mechanical properties of samples produced using laser metal deposition with 316 L stainless steel wire. Optics and Lasers in Engineering. 2017;94:1-11. http://dx.doi.org/10.1016/j.optlaseng.2017.02.008.

[34] Wu W, Xue J, Wang L, Zhang Z, Hu Y, Dong C. Forming process, microstructure, and mechanical properties of thin-walled 316L stainless steel using speed-cold-welding additive manufacturing. Metals. 2019;9(1):109. http://dx.doi.org/10.3390/met9010109.

[35] Preciado WT, Bohorquez CEN. Repair welding of polymer injection molds manufactured in AISI P20 and VP50IM steels. Journal of Materials Processing Technology. 2006;179(1-3):244-250. http://dx.doi.org/10.1016/j.jmatprotec.2006.03.101.

[36] Liang Y, Liu Y, Song Y, Cui W. Optimizing the mechanical properties in the repair zone of 5Cr5MoV by controlling welding heat input. Metals. 2018;8(12):981. http://dx.doi.org/10.3390/met8120981.